Inorg. Chem. **2004**, *43*, 4248–4253

Asymmetric Cationic Coordination Environments in New Oxide Materials: Synthesis and Characterization of $Pb_4Te_6M_{10}O_{41}$ ($M = Nb^{5+}$ or Ta^{5+})

Kang Min Ok and P. Shiv Halasyamani*

Department of Chemistry and Center for Materials Chemistry, 136 Fleming Building, University of Houston, Houston, Texas 77204-5003

Received April 9, 2004

Two new isostructural tellurites, $Pb_4Te_6M_{10}O_{41}$ ($M = Nb^{5+}$ or Ta^{5+}), have been synthesized by standard solid-state techniques using PbO, Nb_2O_5 (or Ta_2O_5), and TeO_2 as reagents. The structures of $Pb_4Te_6Nb_{10}O_{41}$ and $Pb_4Te_6Ta_{10}O_{41}$ were determined by single-crystal and powder X-ray diffraction. The materials exhibit a three-dimensional framework consisting of layers of corner-shared NbO_6 octahedra connected by TeO_3 and PbO_6 polyhedra. The Nb^{5+}, Te^{4+}, and Pb^{2+} cations are in asymmetric coordination environments attributable to second-order Jahn–Teller effects. The Nb^{5+} cations undergo an intraoctahedral distortion either toward a face or a corner, whereas the Te^{4+} and Pb^{2+} cations are in distorted environments attributable to their lone pair. In addition, the TeO_3 polyhedra strongly influence the direction of the Nb^{5+} intraoctahedral distortion. Infrared and Raman spectroscopy, thermogravimetric analysis, and dielectric measurements are also presented. Crystal data: $Pb_4Te_6Nb_{10}O_{41}$, monoclinic, space group *C*2/*m* (No. 12), with $a = 23.412(3)$ Å, $b = 20.114(3)$ Å, $c = 7.5008(10)$ Å, $\beta = 99.630(4)°$, $V = 3482.4(8)$ Å^3, and $Z = 4$; $Pb_4Te_6Ta_{10}O_{41}$, monoclinic, space group *C*2/*m* (No. 12), with $a = 23.340(8)$ Å, $b = 20.068(5)$ Å, $c = 7.472(2)$ Å, $\beta = 99.27(3)°$, $V = 3453.8(2)$ Å^3, and $Z = 4$.

Introduction

The asymmetric cationic coordination environments frequently observed in oxides are often required for a host of materials properties including ferroelectricity, piezoelectricity, dielectric behavior, and second-order nonlinear optical phenomenon.[1−3] Two families of cations are most often observed in asymmetric environments, octahedrally coordinated d^0 transition metals (Ti^{4+}, Nb^{5+}, W^{6+}, etc.) and lone-pair cations (Sn^{2+}, Se^{4+}, Te^{4+}, etc.). With both families, the observed coordination geometry is attributed to second-order Jahn−Teller (SOJT) effects.[4−8] For the octahedrally coordinated d^0 transition metals, SOJT effects occur when the empty *d*-orbitals of the metal mix with the filled *p*-orbitals of the ligands. In extended structures, this mixing results in a host of nearly degenerate electronic configurations that can be removed through the spontaneous distortion of the d^0 transition metal. These distortions can occur along one of three directions, either toward an edge (local C_2 direction), toward a face (local C_3 direction), or toward a corner (local C_4 direction).[9] Thus, bond asymmetries are created within each d^0 transition metal-centered octahedra. The situation with the lone-pair cations is somewhat more complex. Orgel first explained the cationic structural distortion and polarization through the mixing of the metal *s*- and *p*-orbitals.[10] Recently, however, this traditional view of *s*−*p*-orbital mixing has been shown to be incomplete. Watson and Parker,[11,12] Lefebvre et al.,[13,14] and Spaldin and Seshadri[15,16]

* Author to whom correspondence should be addressed. E-mail: psh@uh.edu. Phone: 713-743-3278. Fax: 713-743-2787.

(1) Haertling, G. H. *Electrooptic Ceramics and Devices*; Levinson, L. M., Ed.; Marcel Dekker: New York, 1988; p 371.
(2) Freer, R. *Br. Ceram. Soc. Proc.* **1995**, *55*, 171.
(3) Auciello, O.; Scott, J. F.; Ramesh, R. *Phys. Today* **1998**, *40*, 22.
(4) Bader, R. F. W. *Mol. Phys.* **1960**, *3*, 137.
(5) Bader, R. F. W. *Can. J. Chem.* **1962**, *40*, 1164.
(6) Pearson, R. G. *J. Am. Chem. Soc.* **1969**, *91*, 4947.
(7) Pearson, R. G. *THEOCHEM* **1983**, *103*, 25.
(8) Wheeler, R. A.; Whangbo, M.-H.; Hughbanks, T.; Hoffmann, R.; Burdett, J. K.; Albright, T. A. *J. Am. Chem. Soc.* **1986**, *108*, 2222.
(9) Goodenough, J. B. *Annu. Rev. Mater. Sci.* **1998**, *28*, 1.
(10) Orgel, L. E. *J. Chem. Soc.* **1959**, 3815.
(11) Watson, G. W.; Parker, S. C. *J. Phys. Chem. B* **1999**, *103*, 1258.
(12) Watson, G. W.; Parker, S. C.; Kresse, G. *Phys. Rev. B* **1999**, *59*, 8481.
(13) Lefebvre, I.; Lannoo, M.; Allan, G.; Ibanez, A.; Fourcade, J.; Jumas, J. C. *Phys. Rev. Lett.* **1987**, *59*, 2471.
(14) Lefebvre, I.; Szymanski, M. A.; Olivier-Fourcade, J.; Jumas, J. C. *Phys. Rev. B* **1998**, *58*, 1896.
(15) Seshadri, R.; Hill, N. A. *Chem. Mater.* **2001**, *13*, 2892.
(16) Waghmare, U. V.; Spaldin, N. A.; Kandpal, H. C.; Seshadri, R. *Phys. Rev. B* **2003**, *67*, 125111−1.

10.1021/ic049534h CCC: $27.50
Published on Web 06/05/2004

Table 1. Crystallographic Data for $Pb_4Te_6Nb_{10}O_{41}$

chem formula	$Pb_4Te_6Nb_{10}O_{41}$
fw	3179.46
space group	*C*2/*m* (No. 12)
a (Å)	23.412(3)
b (Å)	20.114(3)
c (Å)	7.5008(10)
β (deg)	99.630(4)
V (Å^3)	3482.4(8)
Z	4
T (°C)	293.0(2)
λ (Å)	0.710 73
ρ_{calcd} (g cm^{-3})	6.064
μ(Mo Kα) (mm^{-1})	27.475
$R(F)^a$	0.0338
$R_w(F_o^2)^b$	0.0902

^{a} $R(F) = \sum||F_o| - |F_c||/\sum|F_o|$. ^{b} $R_w(F_o^2) = [\sum w(F_o^2 - F_c^2)^2/\sum w(F_o^2)^2]^{1/2}$.

have demonstrated that the oxide anion plays an important role in lone-pair formation. Specifically, these researchers argue that the interaction of the *s*- and *p*-orbitals of the metal *with* the oxide anion *p*-states is critical for lone-pair formation. Regardless of how the lone pair is created, its structural consequences are profound, as the lone pair "pushes" the oxide ligands toward one side of the cation, thereby creating a very distorted cationic environment.

As important as these cationic distortions are, controlling their direction, i.e., aligning the distortions in a specific direction, in any solid-state material remains a substantial challenge. To address this challenge, we are investigating materials that contain both types of cations. In addition, we hope to gain a better understanding of how the intraoctahedral distortion of the d^0 transition metal is influenced by the lone-pair cation by examining the various cationic distortions in the materials. In this paper we report the syntheses, structures, and characterization of two new isostructural quaternary oxides, $Pb_4Te_6M_{10}O_{41}$ (M = Nb^{5+} or Ta^{5+}).

Experimental Section

Reagents. PbO (Aldrich, 99+%), Nb_2O_5 (Aldrich, 99.99%), Ta_2O_5 (Alfa Aeser, 99%), and TeO_2 (Aldrich, 99%) were used as received.

Synthesis. $Pb_4Te_6M_{10}O_{41}$ (M = Nb, Ta) were synthesized through standard solid-state techniques. A stoichiometric mixture of PbO (0.893 g, 4.00×10^{-3} mol), Nb_2O_5 (Ta_2O_5) (1.329 g (2.210 g)), 5.00×10^{-3} mol), and TeO_2 (0.958 g, 6.00×10^{-3} mol) was thoroughly ground and pressed into a pellet. The pellet was introduced into a fused silica tube that was evacuated and sealed. The tube was gradually heated to 750 °C (800 °C for $Pb_4Te_6Ta_{10}O_{41}$), held for 24 h, and cooled to room temperature with an intermediate regrinding. Powder X-ray diffraction patterns on the resultant light yellow powders indicated the materials were single phase and in agreement with the generated patterns from the single-crystal data (see Supporting Information). Crystals of $Pb_4Te_6Nb_{10}O_{41}$ were prepared by placing an intimate mixture of PbO (0.223 g, 1.00×10^{-3} mol), Nb_2O_5 (0.133 g, 0.50×10^{-3} mol), and TeO_2 (0.479 g, 3.00×10^{-3} mol) into a gold tube that was subsequently sealed. The gold tube was gradually heated to 800 °C, held for 15 h, and then cooled slowly to 500 °C at 6 °C h^{-1} before being quenched to room temperature. Crystals of $Pb_4Te_6Nb_{10}O_{41}$ (pale yellow blocks; 86% yield based on Nb_2O_5) were recovered with TeO_2 from the tube. Although several attempts were made, all efforts to grow single crystals of $Pb_4Te_6Ta_{10}O_{41}$ under similar reaction conditions produced $PbTeO_3$[17] and a mixture of reagents. Since a pure bulk phase powder of $Pb_4Te_6Ta_{10}O_{41}$ could be synthesized, powder X-ray diffraction was used to demonstrate $Pb_4Te_6Ta_{10}O_{41}$ is isostructural to $Pb_4Te_6Nb_{10}O_{41}$.

Crystallographic Determination. The structure of $Pb_4Te_6Nb_{10}O_{41}$ was determined by standard crystallographic methods. A light yellow block ($0.08 \times 0.10 \times 0.14$ mm^3) was used for single-crystal measurement. Room-temperature intensity data were collected on a Siemens SMART diffractometer equipped with a 1K CCD area detector using graphite-monochromated Mo Kα radiation. A hemisphere of data was collected using a narrow-frame method with scan widths of 0.30° in ω and an exposure time of 30 s/frame. The first 50 frames were remeasured at the end of the data collection to monitor instrument and crystal stabilities. The maximum correction applied to the intensities was <1%. The data were integrated using the Siemens SAINT program,[18] with the intensities corrected for Lorentz, polarization, air absorption, and absorption attributable to the variation in the path length through the detector faceplate. ψ-scans were used for the absorption correction on the hemisphere of data. The data were solved and refined using SHELXS-97 and SHELXL-97, respectively.[19,20] All atoms were

Table 2. Selected Bond Distances (Å) for $Pb_4Te_6Nb_{10}O_{41}$

Nb(1)−O(1)	1.8973(12)	Nb(2)−O(5)	2.031(6)	Nb(3)−O(11)	1.953(6)
Nb(1)−O(2)	2.033(6)	Nb(2)−O(6)	1.889(6)	Nb(3)−O(12)	1.9054(14)
Nb(1)−O(3)	2.119(6)	Nb(2)−O(7)	2.116(6)	Nb(3)−O(13)	1.927(6)
Nb(1)−O(4)	1.911(6)	Nb(2)−O(8)	1.9107(18)	Nb(3)−O(14)	1.933(6)
Nb(1)−O(5)	1.907(5)	Nb(2)−O(9)	1.953(6)	Nb(3)−O(15)	2.164(6)
Nb(1)−O(6)	2.045(6)	Nb(2)−O(10)	2.021(6)	Nb(3)−O(16)	2.016(6)
Nb(4)−O(11)	1.902(6)	Nb(5)−O(4)	2.039(6)		
Nb(4)−O(13)	2.001(6)	Nb(5)−O(9)	1.930(6)		
Nb(4)−O(14)	1.975(6)	Nb(5)−O(16)	1.905(6)		
Nb(4)−O(17)	1.961(6)	Nb(5)−O(17)	1.996(6)		
Nb(4)−O(18)	1.903(2)	Nb(5)−O(20)	1.9132(17)		
Nb(4)−O(19)	2.168(6)	Nb(5)−O(21)	2.087(6)		
Te(1)−O(19)	1.888(6)	Te(2)−O(2)	1.896(6)	Te(3)−O(3)	1.888(6)
Te(1)−O(21)	1.914(6)	Te(2)−O(10)	1.913(6)	Te(3)−O(7)	1.880(6)
Te(1)−O(23)	1.891(6)	Te(2)−O(22)	1.851(6)	Te(3)−O(15)	1.876(6)
Pb(1)−O(4)	2.566(6)	Pb(2)−O(14)	2.738(15) × 2	Pb(3)−O(11)	2.948(11) × 2
Pb(1)−O(6)	2.772(7)	Pb(2)−O(15)	2.822(9) × 2	Pb(3)−O(15)	2.868(9) × 2
Pb(1)−O(13)	2.585(6)	Pb(2)−O(22)	2.491(12) × 2	Pb(3)−O(22)	2.457(9) × 2
Pb(1)−O(16)	2.789(7)	Pb(21)−O(14)	2.803(15)	Pb(31)−O(3)	2.87(2)
Pb(1)−O(17)	2.475(6)	Pb(21)−O(14)	2.817(13)	Pb(31)−O(11)	2.880(17)
Pb(1)−O(23)	2.205(6)	Pb(21)−O(15)	2.61(3)	Pb(31)−O(15)	2.61(2)
		Pb(21)−O(19)	2.758(19)	Pb(31)−O(19)	2.749(16)
		Pb(21)−O(22)	2.451(15)	Pb(31)−O(22)	2.383(13)
		Pb(21)−O(22)	2.506(11)	Pb(31)−O(22)	2.439(12)

Table 3. Powder X-ray Diffraction Data for $Pb_4Te_6Ta_{10}O_{41}$ [Refined Unit Cell[a] $a = 23.340(8)$ Å, $b = 20.068(5)$ Å, $c = 7.472(2)$ Å, $\alpha = 90°$, $\beta = 99.27(3)°$, $\gamma = 90°$; Space Group $C2/m$ (No. 12)]

h	k	l	d_{obs}	d_{calc}	I_{obs}	I_{calc}
1	1	0	15.157	15.131	6	8
2	2	0	7.554	7.566	6	9
1	3	0	6.427	6.424	3	2
4	0	0	5.758	5.759	3	2
0	4	0	5.016	5.017	21	25
2	4	0	4.601	4.600	3	3
6	0	0	3.841	3.839	5	4
−1	1	2	3.674	3.673	6	5
6	2	0	3.585	3.586	14	20
1	1	2	3.496	3.498	11	8
0	6	0	3.345	3.345	100	100
7	1	0	3.246	3.247	63	74
2	2	2	3.183	3.184	38	27
3	1	2	3.097	3.095	44	40
6	4	0	3.047	3.049	11	14
−6	4	1	2.955	2.954	4	1
4	0	2	2.902	2.900	6	5
2	4	2	2.790	2.791	45	30
−1	5	2	2.734	2.735	4	3
1	5	2	2.659	2.660	9	7
7	5	0	2.545	2.545	34	42
3	5	2	2.470	2.469	13	16
−4	6	2	2.371	2.371	3	2
4	6	2	2.192	2.191	4	3
7	7	0	2.161	2.162	8	9
3	7	2	2.114	2.115	13	10
5	9	0	2.008	2.007	8	6

[a] Calculated using the atomic coordinates for $Pb_4Te_6Nb_{10}O_{41}$ but substituting tantalum for niobium.

refined with anisotropic thermal parameters and converged for $I > 2\sigma(I)$. During the refinement, significant residual electron density peaks around Pb(2) and Pb(3) were observed indicating cationic disorder. Thus, Pb(2) and Pb(3) were disordered over two sites with the total occupancies constrained to 1.0 (see Supporting Information). All calculations were performed using the WinGX-98 crystallographic software package.[21] Crystallographic data and selected bond distances for $Pb_4Te_6Nb_{10}O_{41}$ are given in Tables 1 and 2, with additional details found in the Supporting Information.

Powder Diffraction. The X-ray powder diffraction data were collected on a Scintag XDS2000 diffractometer at room temperature (Cu Kα radiation, $\theta-\theta$ mode, flat plate geometry) equipped with Peltier germanium solid-state detector in the 2θ range 3−80° with a step size of 0.01° and a step time of 8 s. For $Pb_4Te_6Ta_{10}O_{41}$, the unit cell was determined by using the program ERACEL.[22] The unit cell, d_{obs}, d_{calc}, I_{obs}, and I_{calc} for $Pb_4Te_6Ta_{10}O_{41}$ are given in Table 3.

Infrared and Raman Spectroscopy. Infrared spectra were recorded on a Matteson FTIR 5000 spectrometer in the 400−4000 cm^{-1} range, with the sample pressed between two KBr pellets. Raman spectra were recorded at room temperature on a Digilab FTS 7000 spectrometer equipped with a germanium detector with the powder sample placed in separate capillary tubes. Excitation was provided by a Nd:YAG laser at a wavelength of 1064 nm, and the output laser power was 544 mW. The spectral resolution was about 4 cm^{-1}, and 200 scans were collected for each sample.

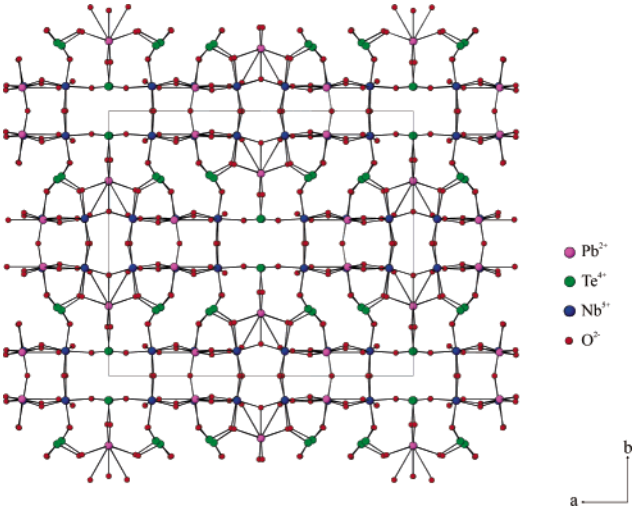

Figure 1. Ball-and-stick diagram of $Pb_4Te_6Nb_{10}O_{41}$ in the *ab*-plane. Note the spaces in the structure where the lone pair on the Te^{4+} cation resides.

Thermogravimetric Analysis. Thermogravimetric analyses were carried out on a TGA 2950 Thermogravimetric Analyzer (TA Instruments). The samples were contained within platinum crucibles and heated at a rate of 10 °C min^{-1} from room temperature to 1000 °C in static air.

Dielectric Characterization. Dielectric constant (κ) measurements were performed using a HP4192A impedance analyzer operating at 1 MHz. Polycrystalline $Pb_4Te_6Nb_{10}O_{41}$ and $Pb_4Te_6Ta_{10}O_{41}$ were pressed into 1.2 cm diameter and 0.15 cm thick pellets and sintered at 700 °C for 24 h. The pellets had a density 90% of theoretical. A conducting silver paste was applied to the pellet surfaces for electrodes and cured at 400 °C. The temperature dependence of the dielectric constants (TCK) was measured, between −20 and 100 °C, by placing the pellets in a Linkam THMSE600 hot stage.

Results and Discussion

Structures. Since both materials are isostructual, only the structural details of $Pb_4Te_6Nb_{10}O_{41}$ will be given. $Pb_4Te_6Nb_{10}O_{41}$ is a new quaternary $Pb^{2+}-Te^{4+}-Nb^{5+}-$ oxide exhibiting a three-dimensional framework structure that consists of layers of corner-shared NbO_6 octahedra connected by asymmetric TeO_3 and PbO_6 polyhedra (see Figure 1). The five unique Nb^{5+} cations are in octahedral coordination bonded to six oxygen atoms. The Nb^{5+} cations undergo out-of-center distortions creating bond asymmetries within each NbO_6 octahedron. These intraoctahedral distortions, however, are not directionally identical. For each unique Nb^{5+} cation, the directions of the distortion are Nb(1)-C_3, Nb(2)-C_3, Nb(3)-C_4, Nb(4)-C_4, and Nb(5)-C_3 (see Figure 2). The Nb−O bond distances range from 1.889(6) to 2.168(6) Å with O−Nb−O bond angles ranging from 79.5(2) to 177.4(3)°. The three unique Te^{4+} cations are in a distorted trigonal pyramid environment, bonded to three oxygen atoms. The Te−O bond distances range from 1.851(6) to 1.914(6) Å with O−Te−O bond angles ranging from 90.9(3) to 100.4(3)°. All of the Te^{4+} cations are in asymmetric coordination environments attributable to their lone pair (see Figure 3). The three unique Pb^{2+} cations are also in asymmetric six-

(17) Sciau, P.; Lapasset, J.; Moret, J. *Acta Crystallogr.* **1986**, *C42*, 1688.
(18) *SAINT, version 4.05*: *Program for Area Detector Absorption Correction*; Siemens Analytical X-ray Instruments: Madison, WI, 1995.
(19) Sheldrick, G. M. *SHELXS-97-A program for automatic solution of crystal structures*; University of Goettingen: Goettingen, Germany, 1997.
(20) Sheldrick, G. M. *SHELXL-97-A program for crystal structure refinement*; University of Goettingen: Goettingen, Germany, 1997.
(21) Farrugia, L. J. *J. Appl. Crystallogr.* **1999**, *32*, 837.
(22) Laugier, J.; Filhol, A. *ERACEL-A program for refinement of the cell parameters*; 1978.

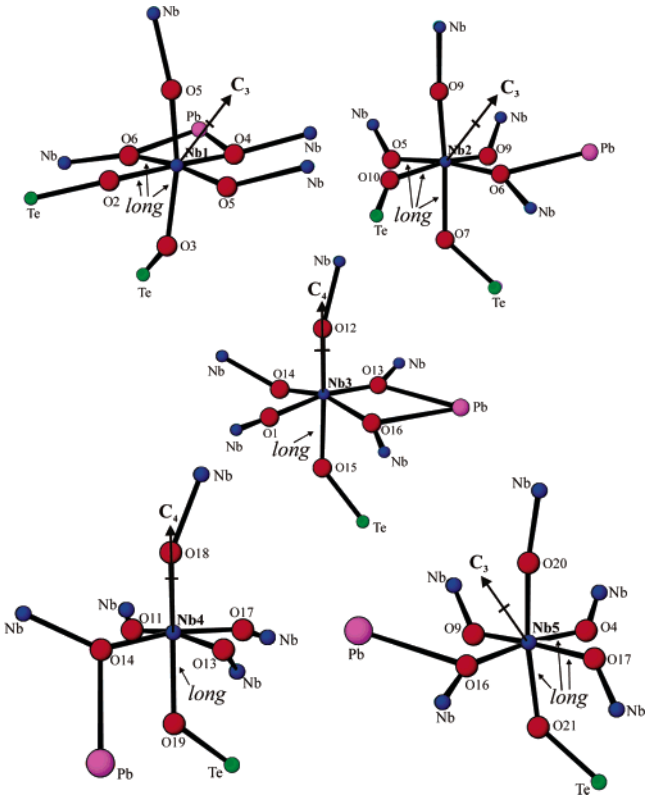

Figure 2. Ball-and-stick diagram of the five unique NbO_6 octahedra in $Pb_4Te_6Nb_{10}O_{41}$. The direction of the out-of-center distortion, and local dipole moment, is represented by an arrow. Note that the direction of the out-of-center distortion is away from the oxygen atom(s) that bridge to a Te^{4+} cation.

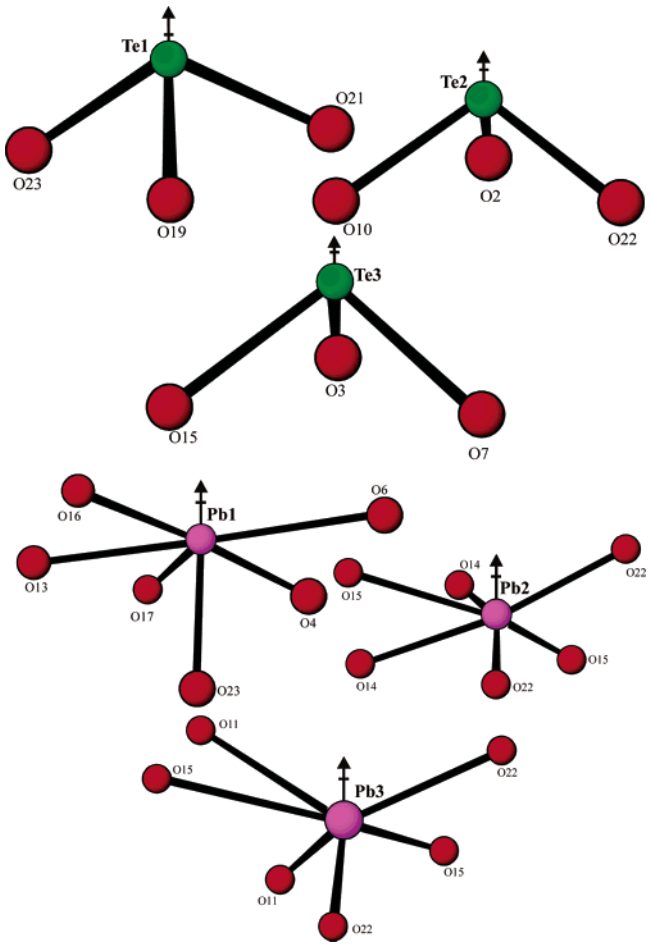

Figure 3. Ball-and-stick diagram of the TeO_3 and PbO_6 asymmetric polyhedra, with the direction of the local dipole moment represented by an arrow.

coordinate environments attributable to their lone pair (see Figure 3). The Pb−O bond distances range from 2.205(6) to 2.948(11) Å with O−Pb−O bond angles ranging from 62.9(4) to 150.4(12)°. Bond valence calculations[23,24] on $Pb_4Te_6Nb_{10}O_{41}$ resulted in values ranging from 1.72 to 2.26, 3.72 to 3.89, and 5.00 to 5.09 for Pb^{2+}, Te^{4+}, and Nb^{5+}, respectively.

Structurally $Pb_4Te_6Nb_{10}O_{41}$ consists of corner-shared NbO_6 octahedra that are further linked to TeO_3 and PbO_6 polyhedra to form a three-dimensional framework (see Figure 1). The "backbone" of the structure may be described as blocks of 2×6 NbO_6 corner-shared octahedra (see Figure 4a). These blocks are observed in the *ab*-plane and are infinite along the [001] direction. The blocks are "capped" along the [010] direction by two TeO_3 and two PbO_6 groups (see Figure 4b). These "capping" polyhedra serve to bridge to similar blocks along the [010] direction. Along the [100] direction the blocks are connected by the third TeO_3 group, to form the three-dimensional framework (see Figure 1). As seen in Figure 1, gaps in the structure are observed in the *ab*-plane wherein the lone pair on the TeO_3 groups reside. If we examine the NbO_6 blocks in the *ac*-plane, we note that four- and six-member "rings" are observed (see Figure 5a). Within the four-member "ring" a chain of corner shared PbO_6 polyhedra are observed running along the [001] direction, whereas within the six-member ring a PbO_6 polyhedron is observed (see Figure 5b). Both PbO_6 polyhedra link to NbO_6 and TeO_3 groups. The manner in which the PbO_6 polyhedra reside within the rings is shown in Figure 5a−c. What is also clear from Figure 5c is the spaces in the *ac*-plane where the Pb^{2+} lone pair resides.

As previously stated, one of our motivations for investigating materials within the Pb^{2+}−Te^{4+}−M^{5+}−oxide (M^{5+} = Nb^{5+} or Ta^{5+}) system was to better understand the influence of the lone-pair cation on the intraoctahedral distortion of the d^0 transition metal. The influence of the lone-pair cation on the out-of-center displacement is a secondary distortive effect, whereas the SOJT effects are the primary distortive effects.[25,26] As previously stated, the d^0 transition metal can distort either toward an edge (C_2), face (C_3), or corner (C_4) of its octahedron. In $Pb_4Te_6Nb_{10}O_{41}$, face- and corner-type distortions are observed with the Nb^{5+} cation. In addition to the intraoctahedral distortion, the Pb^{2+} and Te^{4+} cations are also in asymmetric coordination environments attributable to their lone pair and form distorted PbO_6 and TeO_3 polyhedra. When the distortions are examined more closely, we observe some very interesting trends. Figure 2 shows the unique NbO_6 octahedra along with the metal

(23) Brown, I. D.; Altermatt, D. *Acta Crystallogr.* **1985**, *B41*, 244.
(24) Brese, N. E.; O'Keeffe, M. *Acta Crystallogr.* **1991**, *B47*, 192.
(25) Kunz, M.; Brown, I. D. *J. Solid State Chem.* **1995**, *115*, 395.
(26) Welk, M. E.; Norquist, A. J.; Arnold, F. P.; Stern, C. L.; Poeppelmeier, K. R. *Inorg. Chem.* **2002**, *41*, 5119.

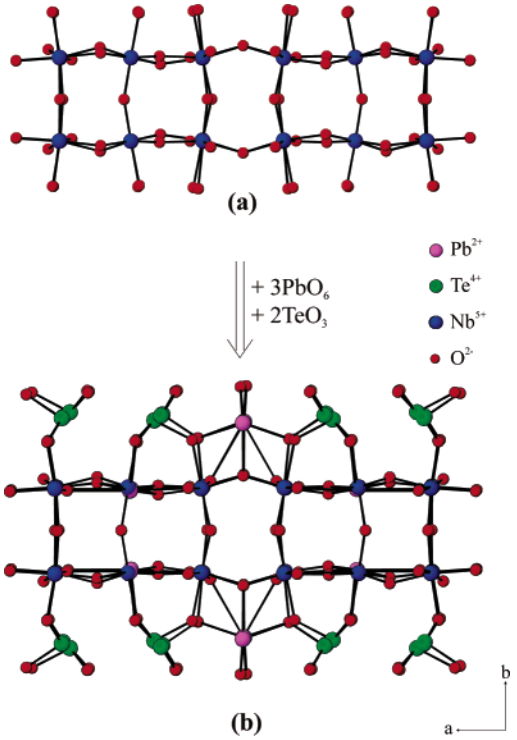

Figure 4. Ball-and-stick representation of the (a) 2×6 NbO_6 octahedral blocks in $Pb_4Te_6Nb_{10}O_{41}$ and (b) addition of 3 PbO_6 and 2 TeO_3 asymmetric polyhedra that "cap" and bridge the blocks.

cation(s) linked to the oxide ligands. The long Nb−O bonds are indicated within each NbO_6 octahedron. In every instance, the direction of the Nb^{5+} out-of-center distortion is *away from* the oxide ligand bonded to a Te^{4+} cation. Recall that the Te^{4+} cation is found as a TeO_3 polyhedron with a lone pair. We suggest that it is the structural rigidity of the TeO_3 polyhedra that reinforces the direction of the Nb^{5+} out-of-center distortion.[27] In other words, the TeO_3 group is already in a predistorted coordination environment. Any further Te^{4+} distortion would result in unfavorable oxide−oxide or oxide−lone-pair interactions; thus, we suggest that the TeO_3 polyhedra serve as "blocking groups". Since the Nb^{5+} cation undergoes an out-of-center distortion attributable to SOJT effects, the direction of the distortion will be away from the blocking group. Thus, the Nb^{5+} cation distorts away from oxide ligands that bridge to the Te^{4+} cations. There are, however, other cationic polyhedra that contain a lone pair, i.e., the Pb^{2+} cation in the PbO_6 groups. In $Pb_4Te_6Nb_{10}O_{41}$, the Nb^{5+} cation distorts toward or away from the oxide ligand(s) bridging to a Pb^{2+} cation. With respect to the secondary distortion alluded to earlier, the influence of the lone-pair cation on the out-of-center distortion of Nb^{5+}, we suggest that the Te^{4+} cation will have a greater influence compared with the Pb^{2+} cation. In other words, the TeO_3 group has more of an affect on the Nb^{5+} out-of-center distortion compared with the PbO_6 group. We suggest this for the following reasons. The TeO_3 polyhedron with its fewer number and shorter range of bond distances and angles, 1.851(6)−1.913(6) Å and 90.9(3)−100.4(3)°, respectively,

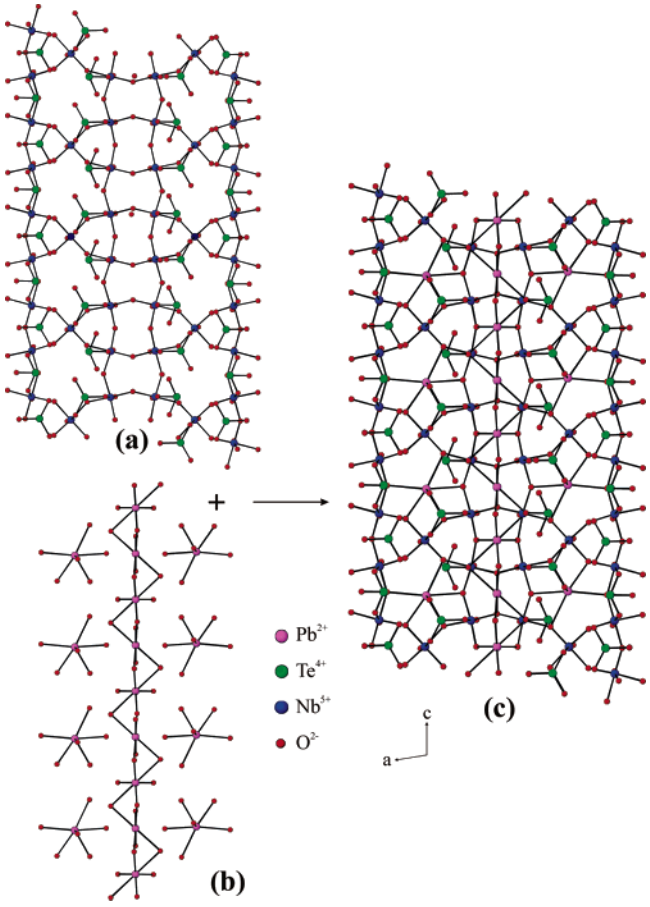

Figure 5. Ball-and-stick representation in the *ac*-plane of (a) NbO_6 and TeO_3 polyhedra revealing four- and six-member "rings", (b) the PbO_6 polyhedra, and (c) the addition of these two substructures to indicate the filling of the "rings".

is more structurally rigid than the PbO_6 group with analogous bond distances and angles of 2.205(6)−2.948(11) Å and 62.9(4)−150.4(12)°, respectively. Thus, the TeO_3 polyhedra are far *less* flexible compared with the PbO_6 polyhedra. Also, on the basis of the Te^{4+} and Pb^{2+} coordination environments (see Figure 3), we notice that the Te^{4+} lone pair is more "directional" than the Pb^{2+} lone pair. This would suggest that the Te^{4+} lone pair has more *p*-orbital character compared with Pb^{2+} lone pair. The relative *s*- and *p*-orbital character of the lone pair could be better quantified by theoretical calculations.

Infrared and Raman Spectroscopy. The infrared and Raman spectra of $Pb_4Te_6M_{10}O_{41}$ (M = Nb or Ta) revealed M−O, Te−O, Pb−O, Pb−O−Te, Pb−O−M, and Te−O−M vibrations. M−O vibrations are observed in both the IR and Raman and occur between 910 and 960 cm^{-1}. Te−O and Pb−O vibrations are also observed in both the IR and Raman and found around 670−770 cm^{-1}. Multiple bands, occurring around 580−630 cm^{-1}, are attributable to M−O−Te and M−O−Pb vibrations. The infrared and Raman vibrations and assignments for $Pb_4Te_6M_{10}O_{41}$ are listed in Table 4. The assignments are consistent with those previously reported.[27−31]

(27) Ok, K. M.; Orzechowski, J.; Halasyamani, P. S. *Inorg. Chem.* **2004**, *43*, 964.
(28) Bart, J. C. J.; Petrini, G. *Z. Anorg. Allg. Chem.* **1980**, *466*, 81.
(29) Gaitan, M.; Jerez, A.; Noguerales, P.; Pico, C.; Veiga, M. L. *Synth. React. Inorg. Met.-Org. Chem.* **1987**, *17*, 479.

Table 4. Infrared and Raman Vibrations for $Pb_4Te_6M_{10}O_{41}$ (M = Nb or Ta)

	M−O	Te−O	Pb−O	Te−O−M	Pb−O−M	Te−O−Pb
			IR (cm^{-1})			
$Pb_4Te_6Nb_{10}O_{41}$	924	768	694	635	587	430
	910	732				416
	563	669				
	524					
$Pb_4Te_6Ta_{10}O_{41}$	928	772	699	636	588	444
	911	739				420
	562	668				
	536					
			Raman (cm^{-1})			
$Pb_4Te_6Nb_{10}O_{41}$	952	794	690	648	586	432
	906	767		621		
	567	725				
	547	667				
$Pb_4Te_6Ta_{10}O_{41}$	960	795	694	636	586	
	910	768				
	548	729				
	520	667				

Thermogravimetric Analysis. The thermal behavior of $Pb_4Te_6M_{10}O_{41}$ (M = Nb or Ta) was investigated using thermogravimetric analysis. $Pb_4Te_6M_{10}O_{41}$ were not stable at higher temperature. In each case a single step decomposition occurs indicating volatilization above 790 °C for $Pb_4Te_6Nb_{10}O_{41}$ and 810 °C for $Pb_4Te_6Ta_{10}O_{41}$. Powder XRD measurements on the calcined materials revealed $Pb_4Te_6M_{10}O_{41}$ ($M = Nb^{5+}$ or Ta^{5+}) decomposed to a mixture of $PbNb_2O_6$ ($PbTa_2O_6$)[32] and unknown amorphous materials.

Dielectric Measurements. Because the reported materials contain polarizable cations, i.e., Pb^{2+}, Te^{4+}, Nb^{5+}, and Ta^{5+}, we thought it would be interesting to investigate their bulk dielectric properties. The dielectric constant for the materials at 1 MHz are $\kappa = 66.05$ and 42.68 for $Pb_4Te_6Nb_{10}O_{41}$ and $Pb_4Te_6Ta_{10}O_{41}$, respectively. With the temperature dependence of the dielectric constant (TCK), the values for $Pb_4Te_6Nb_{10}O_{41}$ and $Pb_4Te_6Ta_{10}O_{41}$ are −404 and −104 ppm/°C (see Table 5). Additional measurements including variable frequency measurements (at 10 kHz, 100 kHz, and 1 MHz) are underway to ascertain the origin of this dielectric behavior.

Table 5. Dielectric Constant (κ), Quality Factor (Q), and Temperature Coefficient of the Dielectric Constant (TCK) for $Pb_4Te_6M_{10}O_{41}$ (M = Nb or Ta) at 1 MHz and 20 °C

	κ	Q (1/tan δ)	TCK[a] (ppm/°C)
$Pb_4Te_6Nb_{10}O_{41}$	66.05	>100	−404
$Pb_4Te_6Ta_{10}O_{41}$	42.68	>100	−104

[a] $TCK = [(\kappa_{100} - \kappa_{-20})/\kappa_{40}]/120$.

Acknowledgment. We thank the Robert A. Welch Foundation for support. This work was also supported by the NSF-Career Program through Grant DMR-0092054, and an acknowledgment is made to the donors of the Petroleum Research Fund, administered by the American Chemical Society, for partial support of this research. P.S.H. is a Beckman Young Investigator. We also acknowledge Jason Locklin and Prof. Rigoberto Advincula for assistance in obtaining the Raman spectra.

Supporting Information Available: X-ray crystallographic files for $Pb_4Te_6Nb_{10}O_{41}$ in CIF format, ORTEP diagrams, and calculated and observed X-ray diffraction patterns for $Pb_4Te_6Nb_{10}O_{41}$ and $Pb_4Te_6Ta_{10}O_{41}$. This material is available free of charge via the Internet at http://pubs.acs.org.

IC049534H

(30) Baltes, M.; Kytokivi, A.; Weckhuysen, B. M.; Schoonheydt, R. A.; Van Der Voort, P.; Vansant, E. F. *J. Phys. Chem. B* **2001**, *105*, 6211.
(31) Porter, Y.; Halasyamani, P. S. *Inorg. Chem.* **2003**, *42*, 205.
(32) Mahe, R. *Bull. Soc. Chim. Fr.* **1966**, *11*, 3401.